



Local impedance spectroscopic and microstructural analyses of Al-in-diffused $\text{Li}_7\text{La}_3\text{Zr}_2\text{O}_{12}$

Jee Hyun Ahn ^a, Seung-Young Park ^a, Jae-Myung Lee ^b, Youngsin Park ^b, Jong-Heun Lee ^{a,*}

^a Department of Materials Science and Engineering, Korea University, Anam-dong, Sungbuk-ku, Seoul 136-713, Republic of Korea

^b Energy Storage Group, Energy Lab, SAIT, Samsung Electronics Co., Ltd., Yongin-Si, Gyeonggi-Do 446-712, Republic of Korea



HIGHLIGHTS

- Li-ion conductivity of Al-in-diffused $\text{Li}_7\text{La}_3\text{Zr}_2\text{O}_{12}$ specimens was measured using local impedance.
- Diffusion of Al into $\text{Li}_7\text{La}_3\text{Zr}_2\text{O}_{12}$ induced abnormal grain growth and formed an intergranular liquid phase.
- Doping of Al stabilized the cubic phase of $\text{Li}_7\text{La}_3\text{Zr}_2\text{O}_{12}$ with a high Li-ion conductivity.
- Single crystals of $\text{Li}_7\text{La}_3\text{Zr}_2\text{O}_{12}$ can be grown via abnormal grain growth.

ARTICLE INFO

Article history:

Received 8 November 2013

Received in revised form

27 December 2013

Accepted 27 December 2013

Available online 8 January 2014

Keywords:

Zirconium-containing lithium garnet

Solid state lithium-ion conductor

All-solid lithium-ion battery

Impedance spectroscopy

Abnormal grain growth

ABSTRACT

A cylindrical $\text{Li}_7\text{La}_3\text{Zr}_2\text{O}_{12}$ specimen in contact with an Al_2O_3 crucible is sintered and the effect of Al diffusion on the microstructure, phase composition, and Li-ion conductivity of $\text{Li}_7\text{La}_3\text{Zr}_2\text{O}_{12}$ is investigated. The decrease in the Li-ion conductivity and Al concentration with increasing distance from the contact area with the Al_2O_3 crucible is confirmed using spatially resolved local-impedance spectroscopy and compositional analysis. The region close to the Al_2O_3 crucible shows abnormally large grains (size > 0.7 mm) within a matrix of fine grains (size: ~ 10 μm), abundant intergranular liquid, the $\text{Li}_7\text{La}_3\text{Zr}_2\text{O}_{12}$ phase mostly in cubic form, and a high Li-ion conductivity (8.5×10^{-5} S cm^{-1}). In contrast, the region far from the Al_2O_3 crucible exhibits uniform fine grains (size: ~ 10 μm), scarce intergranular liquid, the tetragonal form of the $\text{Li}_7\text{La}_3\text{Zr}_2\text{O}_{12}$ phase, and a low Li-ion conductivity (1.1×10^{-6} S cm^{-1}). The incorporation of Al into the $\text{Li}_7\text{La}_3\text{Zr}_2\text{O}_{12}$ lattice and the resulting increase in the number of Li-ion vacancies is suggested to be the main reason for the increase in the Li-ion conductivity. The origins of the abnormal grain growth induced by the diffusion of Al are discussed in relation to the atomic surface structures of $\text{Li}_7\text{La}_3\text{Zr}_2\text{O}_{12}$ and the presence of intergranular liquid phase.

© 2014 Elsevier B.V. All rights reserved.

1. Introduction

$\text{Li}_7\text{La}_3\text{Zr}_2\text{O}_{12}$ (LLZ) with garnet structure is a promising electrolyte material for all-solid-state rechargeable Li-ion batteries on account of its high Li-ion conductivity and chemical stability regarding the use of Li-metal anodes [1–3]. There are tetragonal and cubic phases of garnet-structured LLZ. The ionic conductivity of the cubic phase ($\sim 10^{-4}$ S cm^{-1}) is known to be 2–3 orders of magnitude higher than that of the tetragonal phase (10^{-7} – 10^{-6} S cm^{-1}) [4–7]. The stabilization of the cubic phase, thus, is of critical importance to design a fast solid-state Li-ion conductor.

The aliovalent doping of Al or Ga into LLZ is known to stabilize the cubic LLZ phase [3,8–11] with high Li-ion conductivity by an increase in the Li-vacancy concentration [6,8,12]. In particular, Al is a ubiquitous material that can be easily introduced into LLZ from a ceramic crucible during calcination/sintering, or it can be included during the processing. Note that the doping of Al is known to form an intergranular liquid phase in the presence, or even in the absence, of Si impurities [12] and, it may result in significant variations in the grain size and the chemistry of grain boundaries, which makes the ionic conduction paths of LLZ more complex. Thus, Al doping should be carefully controlled to achieve a reproducible and tunable high Li-ion conductivity.

In the present study, the bottom of a cylindrical LLZ green pellet was in contact with an Al_2O_3 crucible during sintering and the effect of Al diffusion on the microstructures, phases, and electrical properties of LLZ was systematically investigated by spatially

* Corresponding author. Tel.: +82 2 3290 3282; fax: +82 2 928 3584.

E-mail address: jongheun@korea.ac.kr (J.-H. Lee).

resolved measurements of the complex impedance using a millimeter-scale electrode array. Because a single specimen is used for the analyses, the present method can minimize the fluctuations of a number of experimental parameters, such as sintering temperature, evaporation rate of Li, and the composition of the pellet and, thereby, can provide useful information on the diffusion of Al through solid LLZ. The main focus is directed on the elucidation of the role of Al addition on various physical–chemical properties of LLZ.

2. Experimental

LiOH ($\geq 98\%$, Sigma–Aldrich, Inc., USA), La_2O_3 ($\geq 99.9\%$, Sigma–Aldrich, Inc., USA), and ZrO_2 ($\geq 99.0\%$, Kanto Chemical Co., Japan) powders were used as raw materials. In order to remove residual moisture, the La_2O_3 powders were calcined at $900\text{ }^\circ\text{C}$ for 24 h before mixing. 8.7846 g of LiOH powders, 22.1859 g of calcined La_2O_3 powders, and 10.8360 g of ZrO_2 powders were ball-milled for 24 h using 2-propanol as solvent ($\geq 99.5\%$, Samchun Chemical Co., Korea). The molar ratio of $[\text{Li}]/[\text{La}]/[\text{Zr}]$ was set to 7.7:3:2 considering the evaporation of the Li component during sintering at high temperature. The powders were calcined at $900\text{ }^\circ\text{C}$ for 12 h using a zirconia crucible. Note that zirconia crucible was used in the calcination process to avoid any possible Al contamination from the crucible. The powders were dried at $80\text{ }^\circ\text{C}$ for 24 h and pulverized. Subsequently, the powders were ball-milled again for 24 h to eliminate agglomerates.

In order to investigate the effect of Al diffusion from the Al_2O_3 crucible onto the physical–chemical properties of LLZ specimens,

two different kinds of samples were fabricated (Fig. 1). First, two LLZ pellets with and without Al contamination were prepared by uniaxial pressing of 0.6 g of LLZ powders, followed by isostatic pressing at 200 MPa and sintering at different positions within the Al_2O_3 crucible (Fig. 1a). For this, the bottom of one green pellet was directly in contact with the Al_2O_3 crucible and the side and top regions were covered with LLZ powders of the same composition to induce diffusion of Al from the bottom Al_2O_3 crucible and, simultaneously, to prevent contamination from other regions. The other pellet was completely muffled with LLZ powders of the same composition. Two specimens were sintered at $1220\text{ }^\circ\text{C}$ for 18 h. For simplicity, hereinafter, the LLZ specimens sintered with and without contact to the Al_2O_3 crucible are denoted as 'LLZ–Al' and 'LLZ–pure' specimens, respectively. After sintering, electrodes were formed by printing Ag paste (Elcoat P-100, CANS, Japan) and drying.

Second, a cylindrical LLZ specimen was sintered on top of an Al_2O_3 crucible, and the effect of Al diffusion from the Al_2O_3 crucible was studied using spatially resolved investigations of impedance spectra, microstructures, and compositions (Fig. 1b). 2 g of LLZ powders were compacted into a cylindrical green body by uniaxial and isostatic pressing (200 MPa). A cylindrical pellet was placed on the Al_2O_3 crucible and the other side (top regions) was covered with LLZ powders of the same composition. The specimen was sintered at $1220\text{ }^\circ\text{C}$ for 18 h. A slab with a size of $5.1 \times 9.5 \times 1.0\text{ mm}^3$ was obtained by cutting the cylindrical, Al-in-diffused sintered specimen (diameter: 5.1 mm, height: 9.5 mm) along the diameter. After polishing the surface on each side of the slab (thickness: 1.0 mm), 5 electrodes ($2 \times 1\text{ mm}^2$) were made on both surfaces along the long side of the sample from the Al-rich bottom to the

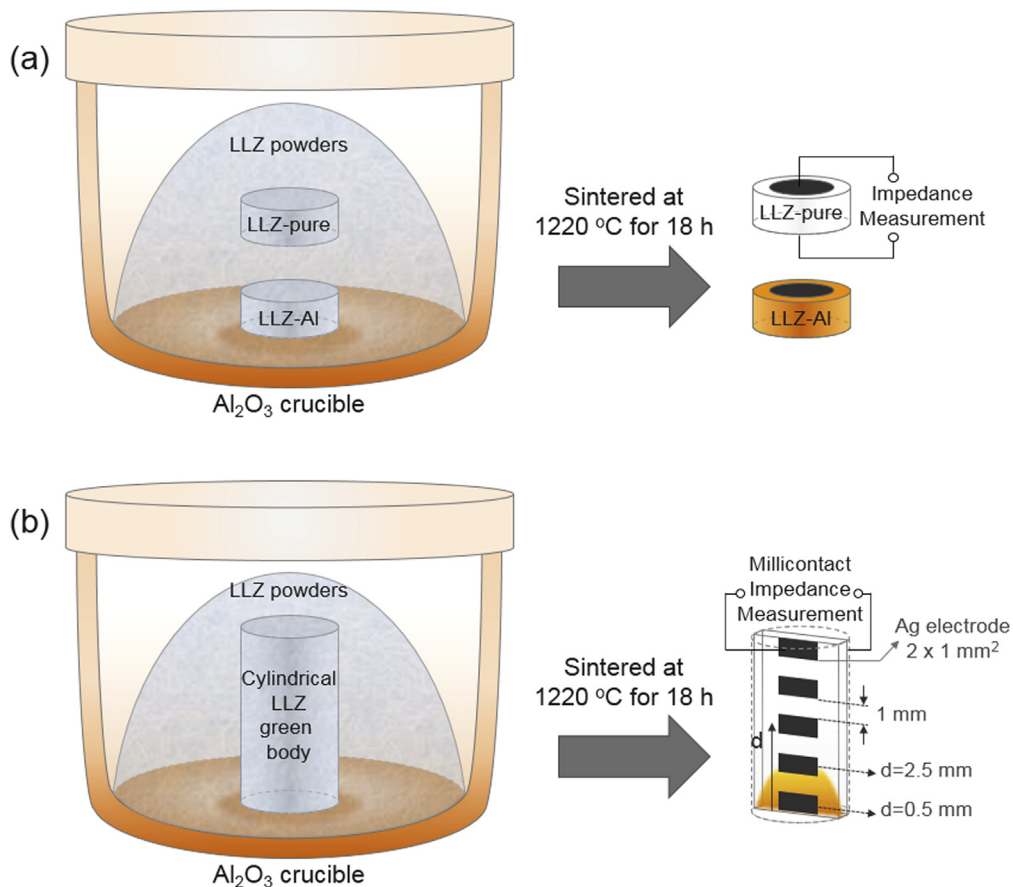


Fig. 1. Experimental procedures: (a) two LLZ pellet specimens with and without contact with an Al_2O_3 crucible during sintering; (b) a cylindrical specimen on an Al_2O_3 crucible for local impedance measurements (right).

other side with 1.0-mm spacing (Fig. 1b), fabricated by screen-printing Ag paste and drying.

The complex impedance was measured at 25 °C using a dielectric analyzer (Alpha-N, Novocontrol, Germany) covering a frequency range of 10^{-1} – 10^7 Hz. The bias voltage of 0.3 V was used for impedance measurement. The microstructures and compositions of the LLZ specimens were compared and investigated using scanning electron microscopy (SEM, Hitachi S-4300, Hitachi, Japan) with energy-dispersive X-ray spectroscopy (EDS, Horiba EX-200, Horiba, Japan). The crystal structures were analyzed using X-ray powder diffraction (XRD, D/Max-2500C, Rigaku, Japan). The concentration of the elements was investigated using electron probe micro-analysis (EPMA, JXA-8500F, JEOL Co., Japan).

3. Results and discussion

Complex impedance spectra of LLZ-Al and LLZ-pure specimens were measured at 25 °C, shown in Fig. 2. Both impedance spectra consist of two contributions, the first originating from electrode polarization at low frequencies and the second corresponding to the total contribution of the sample material at high frequencies. No distinctive semicircle arising from grain boundaries was observed, indicating difficulties for the deconvolution of the total contribution of the sample into components originating from the grain interior and the grain boundaries. The total resistivity (ρ_{total}) of the LLZ-Al specimen was 3.5 kΩ cm (Fig. 2a), which is significantly lower than that of the LLZ-pure specimen (318.3 kΩ cm) (Fig. 2b). Based on XRD measurements, the LLZ-Al specimen was identified to be cubic LLZ phase (Fig. 3a) while, additionally, the tetragonal phase was observed in LLZ-pure specimens (arrows in Fig. 3b). These results indicate that the phase composition and Li-ion conductivity of LLZ specimens is strongly depend on the Al contamination originating from the Al_2O_3 crucible.

In order to investigate the effect of Al doping from the crucible onto the physicochemical properties of the LLZ specimens, a cylindrical specimen was placed on an Al_2O_3 crucible and sintered at 1220 °C for 18 h. The spatially resolved impedance spectra of a thin slab were measured at various distances from the Al_2O_3 crucible. The measurement geometry is illustrated in Fig. 1b and the corresponding impedance spectra are presented in Fig. 4. The semicircles arising from the total contribution become larger as the distance from the contact of Al_2O_3 crucible (d) increased from 0.5 mm to 8.5 mm. The values of ρ_{total} were calculated from the impedance spectra, and the results are plotted in Fig. 5a. The ρ_{total} values at

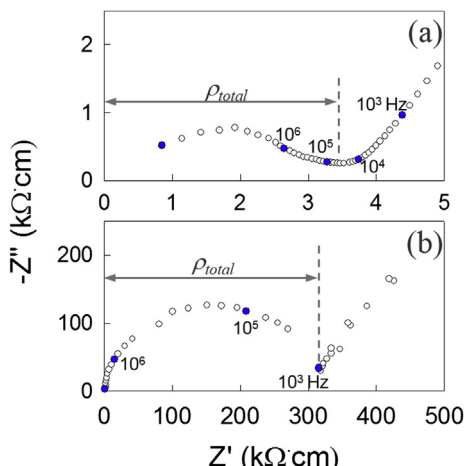


Fig. 2. Complex impedance spectra of (a) LLZ-Al and (b) LLZ-pure specimens at 25 °C.

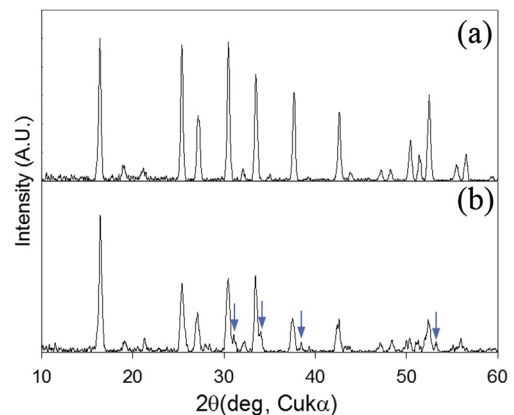


Fig. 3. XRD patterns of (a) LLZ-Al and (b) LLZ-pure specimens (arrows indicate of the tetragonal phase).

$d = 0.5$ mm and 2.5 mm were 11.7 and 180.2 kΩ cm, respectively, which increased up to 901.8 kΩ cm at $d = 8.5$ mm.

The spatial distribution of the Al concentration in the specimen was determined by EPMA mapping (Fig. 5b). Note that the Al contents at the nominal positions of $d = 1.0, 2.5, 4.0, 5.5, 7.0$, and 8.5 mm were measured by averaging over a range of ± 0.5 mm. It clearly shows that a substantial amount of Al diffused from the

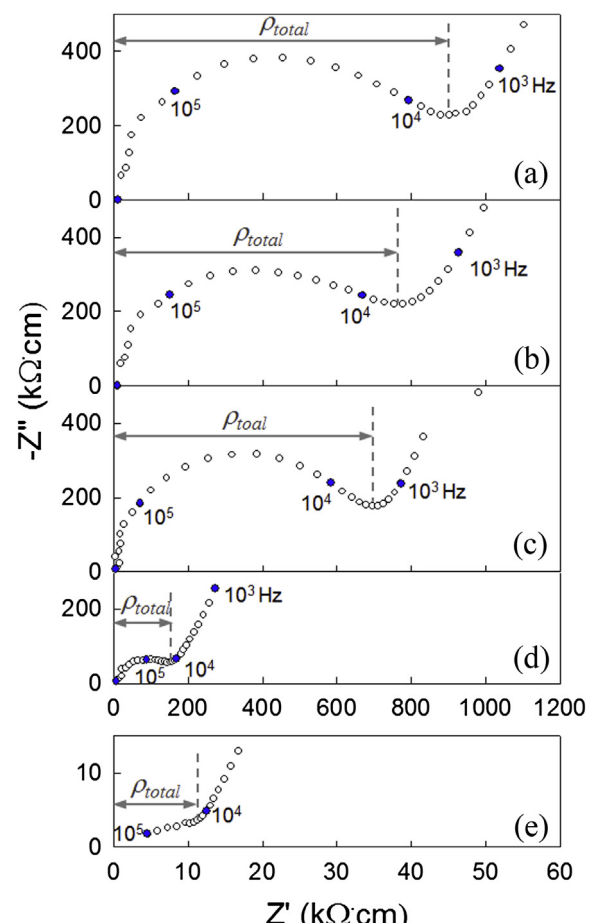


Fig. 4. Complex impedance spectra of Al-in-diffused specimens at 25 °C (d = distance from the contact area with the Al_2O_3 crucible) (a) $d = 8.5$ mm, (b) $d = 6.5$ mm, (c) $d = 4.5$ mm, (d) $d = 2.5$ mm, and (e) $d = 0.5$ mm.

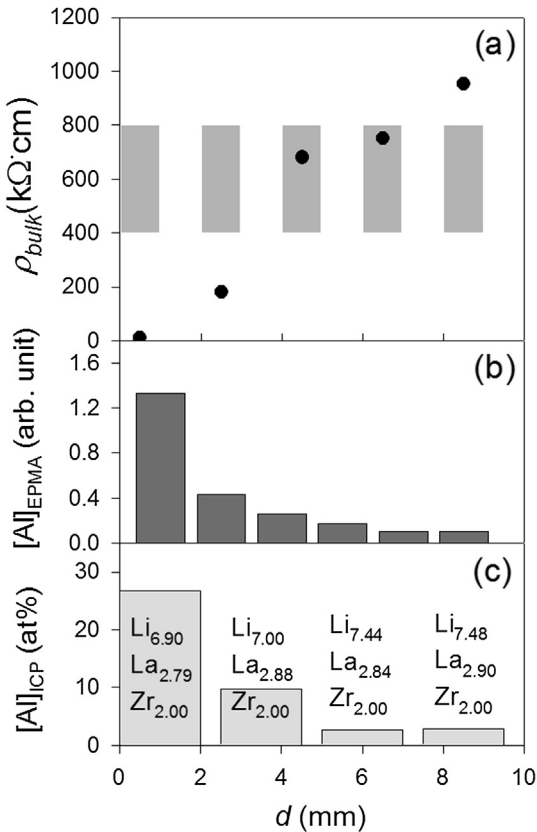


Fig. 5. (a) The ρ_{total} values as calculated from Fig. 4, (b) Al concentration determined from EPMA analysis ($[\text{Al}]_{\text{EPMA}}$), and (c) the composition of LLZ (see the text within figure) and concentration of Al ($[\text{Al}]_{\text{ICP}}$ (at%)) determined from ICP analysis as a function of distance from the contact zone with the Al_2O_3 crucible. The width of each bar in b and c represents the thickness of specimen for compositional analysis.

Al_2O_3 crucible and the concentration of Al decreases as d increases. The composition of LLZ and Al concentration ($[\text{Al}] / ([\text{Al}] + [\text{LLZ}])$) as a function of d were further analyzed using ICP-AES (Fig. 5c). In this analysis, the compositions at the nominal positions of $d = 1.0, 3.5, 6.0, 8.5$ mm were measured by averaging over a range of ± 1.0 mm under assuming that $[\text{Zr}]$ is constant. The diffusion of Al component from the Al_2O_3 crucible was confirmed again by the decrease of Al concentration with increasing d . The $[\text{Al}] = 26.7$ at% to show the high Li-ion conductivity in the present study is consistent with literature that $[\text{Al}] > 20.4$ at% is necessary to stabilized cubic LLZ phase with high ionic conductivity [8]. Note that $[\text{Li}]$ near Al_2O_3 crucible is relatively low, indicating that the evaporation of Li component due to the formation of Li-containing intergranular liquid phase. The sintered LLZ specimens were cut into two pellets at the position of $d = 3.5$ mm and the phases of two specimens were analyzed by XRD (Fig. 6). The pellet that had been in contact with Al_2O_3 during sintering ($0 < d < 3.5$ mm) was identified to be mostly cubic structure (Fig. 6a) containing a small additional amount of the tetragonal phase (indicated by arrows in Fig. 6a). In contrast, the tetragonal phase has been observed in the LLZ pellet far from the contact area with Al_2O_3 ($3.5 < d < 9.0$ mm) (arrows in Fig. 6b). These two experiments clearly show that Al diffused from the Al_2O_3 crucible into the bulk of the LLZ specimen during sintering, and the doping of Al decreases the ρ_{total} value and changes the crystal structure from tetragonal to cubic.

The effect of Al-diffusion on the microstructures of LLZ specimens also has been investigated. Interestingly, near the contact zone of the Al_2O_3 crucible ($0 < d < 1.0$ mm), abnormally large grains

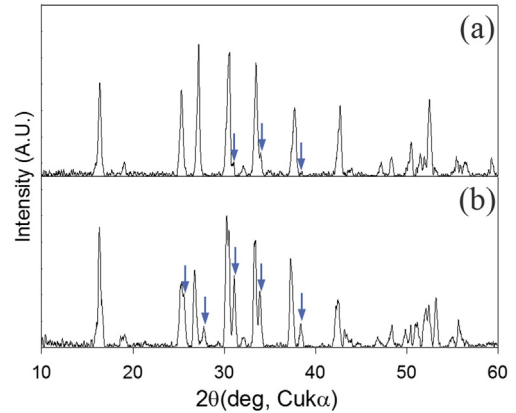


Fig. 6. XRD patterns of a specimen (a) near the contact zone with the Al_2O_3 crucible ($0 < d < 3.5$ mm) and (b) far from the contact area with the Al_2O_3 crucible ($3.5 < d < 9$ mm). Arrows indicate the presence of the tetragonal phase.

with a size of >0.7 mm (see the grains with dotted lines in Fig. 7a) were observed in a matrix of very fine grains (size: $\sim 10 \mu\text{m}$). The abnormal grain growth (AGG) has been confirmed by the clearer image of these grains observed by backscattered electrons (Fig. 7b). No AGG was observed in the region of $d > 1.5$ mm. The reproducibility of the AGG behavior at $0 < d < 1.5$ mm was confirmed by

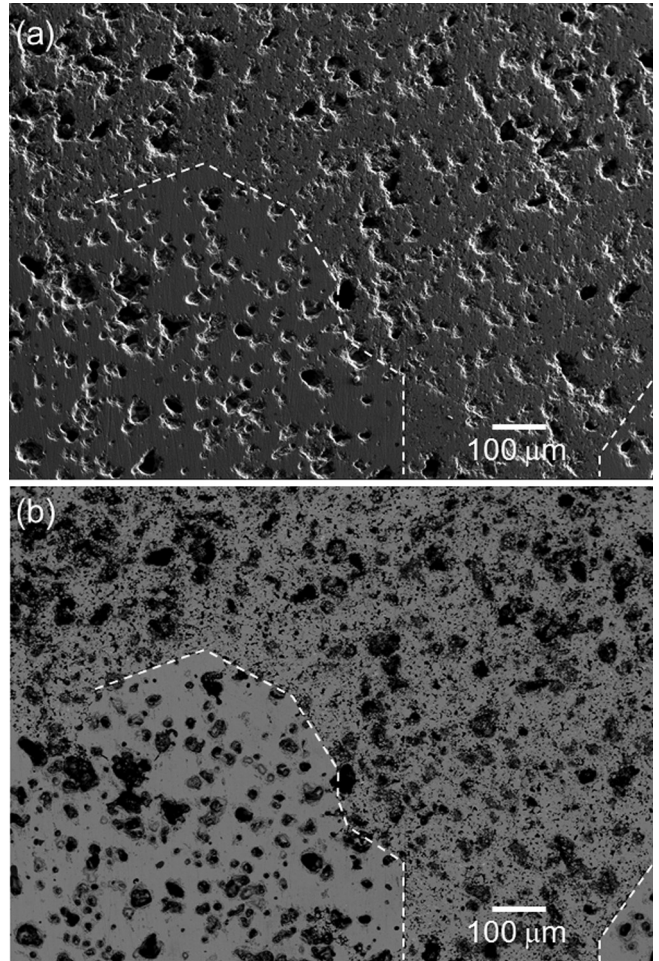


Fig. 7. (a) SEM and (b) backscattered images of a specimen showing a region close to the contact area with the Al_2O_3 crucible ($0 < d < 1.5$ mm).

corresponding observations of a few more specimens (data not shown), indicating that doping of Al into LLZ induces AGG.

The distributions of the elements Al, La, and Zr were analyzed by EPMA mapping (Fig. 8). Both La and Zr components were uniformly distributed over the entire specimen, regardless of AGG (Fig. 8c and d). In contrast, a relatively low Al concentration has been observed within an abnormally large grain (Fig. 8b). The phase and crystal structure of abnormally large grains might be different from those of the small-grain matrix. The predominance of the cubic phase near the Al_2O_3 crucible (Fig. 3a and 6a), however, cannot be understood if the very large grains are tetragonal phase. In this perspective, it is plausible that both small and abnormally large grains are cubic. This indicates that the Al component was also incorporated into the LLZ lattice of the abnormally large grains, which is again supported by the report that the cubic phase of LLZ is stabilized by doping of ~20 at% of Al [8]. A similar concentration of Al is also thought to be incorporated into the LLZ lattice of the small-grain matrix. The Li and Al components in the presence, or even in the absence, of siliceous impurities are known to form an intergranular liquid phase at a temperature as low as ~1055 °C [13] with a composition between Li_5AlO_4 and LiAlO_2 . Although the overall Li concentration in the present study is lower than 50.0 at% (LiAlO_2) and 83.3 at% (Li_5AlO_4), the formation of a Li-containing intergranular liquid phase at a sintering temperature of 1220 °C seems to be plausible considering the abundance of the Li component in the intergranular regions, as well as local heterogeneities of the Li distribution. Thus, the relatively higher Al concentration in the matrix of small grains can be attributed to the intergranular liquid phase consisting of Li, Al, and other components.

In general, AGG, the growth of a limited number of grains to an extraordinary size at the expense of fine matrix grains, occurs when the grain growth is controlled by 2-D nucleation on a singular grain

with atomically smooth interface structures [14], while normal grain growth occurs in spherical grains with atomically rough interface structures when the growth process is controlled by diffusion. Accordingly, the shapes of grains determined by atomic interface structures play the key role in grain growth behaviors. It is observed that an interface of the abnormally large grain (see dotted lines and arrows in Fig. 7) forms a straight line, suggesting that the surface of the cubic LLZ grain in the present study is atomically smooth. The presence of an intergranular liquid phase is also known to accelerate the AGG via fast mass transport [15–17]. The region near the Al_2O_3 crucible showed an abundant amount of the intergranular liquid phase while that far from the Al_2O_3 crucible did not. Accordingly, the AGG observed in the region near the contact zone with the Al_2O_3 crucible can be attributed to both, atomically smooth interfaces and the presence of liquid phases containing Al.

In the region far from the contact area with the Al_2O_3 crucible, tetragonal grains with scarce amounts of the intergranular liquid phases were found. The absence of AGG in this region might be explained on the basis of atomically rough interface structures of the tetragonal phase or by slow grain-growth kinetics due to the absence of an intergranular liquid phase, in spite of atomically smooth interface structures. Thus, at this moment, it is unclear whether the interface structure of the tetragonal phase is atomically smooth or rough. This point needs further clarification.

The higher conductivity of the Al-containing LLZ should be understood in terms of grain-interior and grain-boundary conduction. It has been suggested that the incorporation of Al^{3+} ions at Li^+ sites enhances the Li-ion conductivity not only by a transformation of the crystal structure from anisotropic tetragonal to isotropic cubic, but also by an increase in Li-ion vacancies [3,6,8,9,12]. On the other hand, Kumazaki et al. [4] suggested that the presence of Al along with certain impurities formed a highly Li-ion conducting intergranular liquid phase. If the enhanced Li-ion

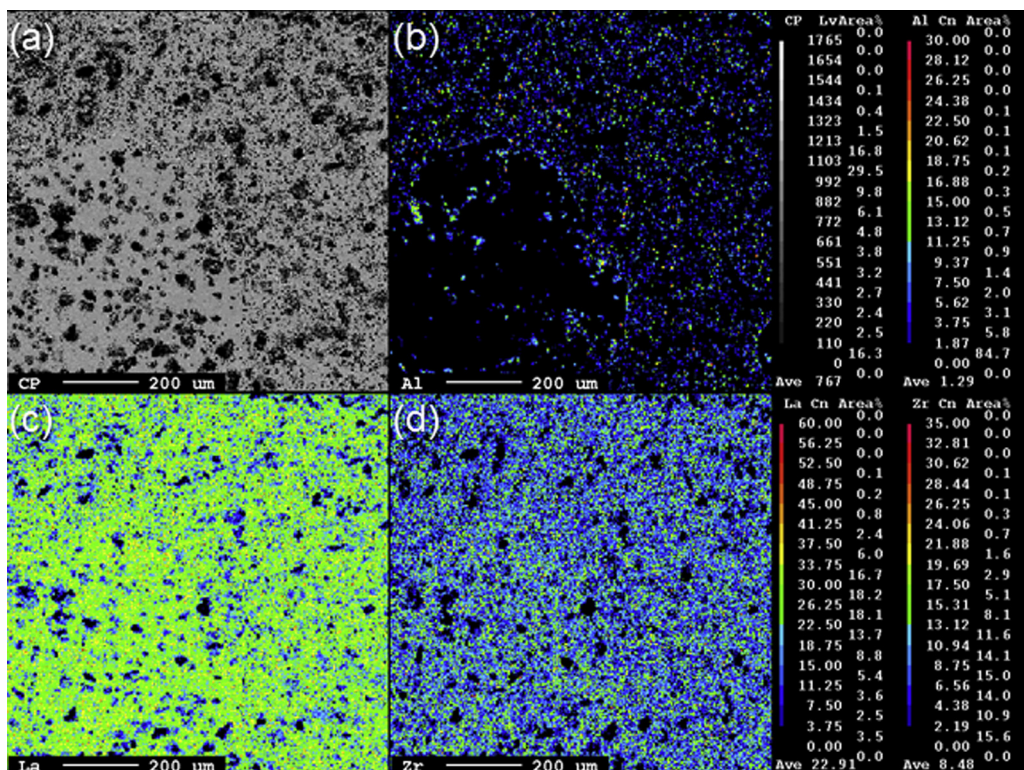


Fig. 8. EPMA elemental mapping of the region shown in Fig. 7: (a) backscattered image; (b) Al; (c) La, and (d) Zr distribution.

conductivity along the Al-containing intergranular phase is the major reason for the high Li-ion conductivity of Al-containing LLZ specimens in the present study, the impedance at the second electrode ($d = 2.5$ mm) consisting of uniform small grains and Al-containing intergranular phase should be significantly higher than that at the first electrode ($d = 0.5$ mm) containing abnormally large grains. The impedance data, however, show the opposite results. This indicates that the stabilization of the cubic structure and the generation of Li-ion vacancies by Al incorporation represent a more plausible explanation than the fast Li-ion conduction through the intergranular liquid phase.

AGG is a facile method to grow oxide single crystals using a simple sintering procedure and relatively large grains can be harvested when the nucleation and growth are tuned precisely [18,19]. Indeed, Geiger et al. [12] reported that LLZ single crystals with the size of up to ~ 100 μm can be grown when the specimen was sintered using a ceramic crucible, while a fine-grained LLZ polycrystalline specimen was prepared by sintering using a Pt crucible. The Al content of the LLZ single crystal was determined to be 1.16 wt% (17.6 at%) by laser ablation inductively coupled plasma mass spectroscopy. These results are consistent with the present findings that the diffusion of Al is the major reason for the occurrence of AGG and the stabilization of the cubic phase in LLZ. Moreover, if the Li-ion conductivity of a large, cubic, Al-doped LLZ crystal, grown by solid-state reaction, is measured and compared with that of polycrystalline LLZ with an identical composition, the role of grain-interior or grain-boundary conduction for the enhancement of the overall Li-ion conductivity can be understood.

4. Conclusions

The effect of Al diffusion from an Al_2O_3 crucible into LLZ during sintering on the microstructure, phase composition, and Li-ion conductivity of LLZ is investigated using SEM, XRD, and spatially resolved, local impedance spectroscopy. The diffusion of Al into LLZ stabilized the cubic crystal structure, induces AGG, formed an intergranular liquid phase, and enhances the Li-ion conductivity by up to ~ 100 times. The angular morphologies of abnormally large LLZ grains reflect the atomically smooth interface structures and the intergranular phase can provide the paths for fast mass transport during grain growth. Thus, the 2-D nucleation and growth have been suggested as a plausible reason to induce AGG in Al-rich

LLZ, in contact with the Al_2O_3 crucible. Moreover, the tuning of the nucleation and growth rate during solid-state sintering can be used to grow large LLZ crystals. The incorporation of Al into the LLZ lattice and the resulting increase in the Li-ion vacancy concentration are suggested as a plausible reason to explain the enhancement of the Li-ion conductivity of LLZ.

Acknowledgments

This work was supported by the National Research Foundation of Korea (NRF) grant funded by the Korea government (MEST) (No. 2013R1A2A1A01006545).

References

- [1] R. Murugan, V. Thangadurai, W. Weppner, *Angew. Chem. Int. Ed.* **46** (2007) 7778–7781.
- [2] M. Kotobuki, H. Munakata, K. Kanamura, Y. Sato, T. Yoshida, *J. Electrochem. Soc.* **157** (2010) A1076–A1079.
- [3] K.-H. Kim, Y. Iriyama, K. Yamamoto, S. Kumazaki, T. Asaka, K. Tanabe, C.A.J. Fisher, T. Hirayama, R. Murugan, Z. Ogumi, *J. Power Sources* **196** (2011) 764–767.
- [4] S. Kumazaki, Y. Iriyama, K.-H. Kim, R. Murugan, K. Tanabe, K. Yamamoto, T. Hirayama, Z. Ogumi, *Electrochim. Commun.* **13** (2011) 509–512.
- [5] J. Awaka, N. Kijima, H. Hayakawa, J. Akimoto, *J. Solid State Chem.* **182** (2009) 2046–2052.
- [6] E.A. Il'ina, O.L. Andreev, B.D. Antonov, N.N. Batalov, *J. Power Sources* **201** (2012) 169–173.
- [7] I. Kokal, M. Somer, P.H.L. Notten, H.T. Hintzen, *Solid State Ionics* **185** (2011) 42–46.
- [8] E. Rangasamy, J. Wolfenstine, J. Sakamoto, *Solid State Ionics* **206** (2012) 28–32.
- [9] Y. Jin, P.J. McGinn, *J. Power Sources* **196** (2011) 8683–8687.
- [10] J. Wolfenstine, J. Ratchford, E. Rangasamy, J. Sakamoto, J.L. Allen, *Mater. Chem. Phys.* **134** (2012) 571–575.
- [11] H.E. Shinawi, J. Janek, *J. Power Sources* **225** (2013) 13–19.
- [12] C.A. Geiger, E. Alekseev, B. Lazic, M. Fisch, T. Armbruster, R. Langner, M. Fechtelkord, N. Kim, T. Pettke, W. Weppner, *Inorg. Chem.* **50** (2011) 1089–1097.
- [13] L.P. Cook, E.R. Plante, *Ceram. Trans.* **27** (1992) 193.
- [14] W. Jo, D.-Y. Kim, N.-M. Hwang, *J. Am. Ceram. Soc.* **89** (2006) 2369–2380.
- [15] S.-H. Hong, D.-Y. Kim, *J. Am. Ceram. Soc.* **84** (2001) 1597–1600.
- [16] J.H. Ahn, J.-H. Lee, S.-H. Hong, N.-M. Hwang, D.-Y. Kim, *J. Am. Ceram. Soc.* **86** (2003) 1421–1423.
- [17] K.-M. Kim, S.-J. Kim, J.-H. Lee, D.-Y. Kim, *J. Eur. Ceram. Soc.* **27** (2007) 3991–3995.
- [18] H.-Y. Lee, J.-S. Kim, D.-Y. Kim, *J. Eur. Ceram. Soc.* **20** (2000) 1595–1597.
- [19] C. Wang, Y.-D. Hou, H.-Y. Ge, M.-K. Zhu, H. Yan, *J. Eur. Ceram. Soc.* **30** (2010) 1725–1730.